Superconducting Bi_2Te: Pressure-induced universality in the $(Bi_2)_m(Bi_2Te_3)_n$ series

Ryan L. Stillwell,[1] Zsolt Jenei,[2] Samuel T. Weir,[2] Yogesh K. Vohra,[3] and Jason R. Jeffries[1]
[1]*Materials Science Division, Lawrence Livermore National Laboratory, Livermore, California 94550, USA*
[2]*Physics Division, Lawrence Livermore National Laboratory, Livermore, California 94550, USA*
[3]*Department of Physics, University of Alabama at Birmingham, Birmingham, Alabama 35294, USA*
(Received 9 November 2015; revised manuscript received 20 February 2016; published 9 March 2016)

Using high-pressure magnetotransport techniques we have discovered superconductivity in Bi_2Te, a member of the infinitely adaptive $(Bi_2)_m(Bi_2Te_3)_n$ series, whose end members, Bi and Bi_2Te_3, can be tuned to display topological surface states or superconductivity. Bi_2Te has a maximum $T_c = 8.6$ K at $P = 14.5$ GPa and goes through multiple high-pressure phase transitions, ultimately collapsing into a bcc structure that suggests a universal behavior across the series. High-pressure magnetoresistance and Hall measurements suggest a semimetal to metal transition near 5.4 GPa, which accompanies the hexagonal to intermediate phase transition seen via x-ray diffraction measurements. In addition, the linearity of $H_{c2}(T)$ exceeds the Werthamer-Helfand-Hohenberg limit, even in the extreme spin-orbit scattering limit, yet is consistent with other strong spin-orbit materials. Considering these results in combination with similar reports on strong spin-orbit scattering materials seen in the literature, we suggest the need for a new theory that can address the unconventional nature of their superconducting states.

DOI: 10.1103/PhysRevB.93.094511

I. INTRODUCTION

The past several years have seen a large volume of research dedicated to materials whose properties are driven by the topology of their quantum states [1]. These states realize long theorized exotic quantum-mechanical effects, such as Weyl fermions, predicted nearly a century ago [2,3], and others, such as topological insulators (TIs) and topological superconductors, predicted only a few years ago [4,5]. One of the more exciting prospects of TIs is that with proximity-induced superconductivity [6] they provide the Z_2 nontrivial state allowing for promising applications in spintronics and quantum computation [7] as well as the experimental realization of Majorana fermions [8].

One of the key properties necessary for making a TI is strong spin-orbit coupling, first discovered in HgTe quantum wells and later found in several bismuth-based chalcogenides [9–12]. A particularly interesting family of these materials is the infinitely adaptive series $(A_2)_m(A_2Q_3)_n$ with $A = (\mathrm{Bi,Sb})$ and $Q = (\mathrm{Se,Te})$. Although members of this series are well known as some of the best thermoelectric materials, they were recently found to be topological insulators as well [13–16]. In particular, the end members of the infinitely adaptive $(Bi_2)_m(Bi_2Te_3)_n$ series, Bi and Bi_2Te_3, can be experimentally tuned to display topological surface states or superconductivity under appropriate conditions [11,17–19].

In our search for functional materials that possess these exotic properties we synthesized and studied Bi_2Te, a member of the $(Bi_2)_m(Bi_2Te_3)_n$ series, with $m = 2$ and $n = 1$. Containing a Bi fraction of 0.67, Bi_2Te is on the Bi-rich side of this series, which spans the spectrum from pure Bi ($m = 3 : n = 0$) to Bi_2Te_3 ($m = 0 : n = 3$). Similar to other members of this series [20–22], Bi_2Te transforms from an ambient pressure semimetal to a high-pressure superconductor, progressing through multiple structural and electronic phases, including a high-pressure body-centered-cubic (bcc) structure with a maximum $T_c = 8.6$ K at 14.5 GPa. This suggests a universal behavior seen across the $(Bi_2)_m(Bi_2Te_3)_n$ homologous series as well as in elemental Te [23,24], Se [25], and Bi_2Se_3 [26,27].

II. EXPERIMENT

Single crystals of Bi_2Te were grown using the self-flux method. Elemental Bi and Te (99.999%, ESPI Metals) in a ratio of 12 at.% Te and 88 at.% Bi were combined in an alumina crucible and sealed under 500 mbars of high-purity argon gas in a quartz tube and melted at 420 °C for 2 days. The solution was then cooled to 318 °C over a period of 4 days at which point the quartz tube was removed from the oven and centrifuged to remove excess flux. Large platelets were removed and ground into a coarse powder using a mortar and pestle. The coarse powder was then placed on a glass slide and chopped with a razor blade into a fine powder for powder x-ray-diffraction characterization. These measurements confirmed that the lattice parameter is consistent with literature and that they were single phase Bi_2Te [13]. Additionally, we did not observe any peak-broadening effects that might be expected if there were any core-shell crystals indicating compositional gradients.

For structural studies under pressure we used a conventional membrane-driven diamond-anvil cell (DAC) with 300-μm diamond culets. The powdered Bi_2Te, 3–5-μm particle size, was loaded into a 130-μm-diameter sample chamber that was drilled out of a rhenium gasket preindented to 25 GPa, corresponding to an initial thickness of 23 μm. The chamber was also loaded with fine copper powder (3–6 μm, Alfa Aesar) as the pressure calibrant and neon, precompressed to 30 000 psi, as the pressure-transmitting medium. Room-temperature angle-dispersive x-ray-diffraction experiments were performed at HPCAT (beamline 16 BM-D) at the Advanced Photon Source at Argonne National Laboratory. The sample was illuminated with a 29.2-keV monochromatic x-ray beam, and angular-dispersive diffraction patterns were collected with a PerkinElmer detector using an exposure time of 10–20 s. The two-dimensional diffraction images were integrated using FIT2D [28], then analyzed using the JADE software package to extract crystal structure and volume information. To determine the pressure, we used the Vinet equation of state of the copper with fitting parameters for

the bulk modulus $B_0 = 133$ GPa and its pressure derivative $B_0' = 5.01$ from Dewaele *et al.* [29].

For electrical transport studies under pressure we used an eight-probe designer DAC [30,31] with 280-μm-diameter culets, steatite as a pressure-transmitting medium, and ruby as the pressure calibrant [32,33]. A MP35N metal gasket was preindented to an initial thickness of 60 μm, and a 120-μm hole was drilled in the center of the indentation for the sample chamber using an electric discharge machine. A small crystal of Bi_2Te with dimensions of 80-μm diameter and 10-μm thick was taken out of the larger micaceous crystallites and placed onto the designer anvil to ensure electrical contact with the tungsten leads exposed on the face of the designer diamond culet. Pressure was measured at room temperature on two separate ruby spheres within the sample chamber in order to estimate pressure distribution across the chamber. Based on previous studies using this type of DAC the error in the pressure at low temperatures was estimated to be 5% [31]. The temperature was measured using a calibrated Cernox thermometer affixed to the outside of the DAC. Electrical transport measurements were performed as a function of temperature and magnetic field using the ac transport option in the Quantum Design physical property measurement system.

III. RESULTS

High-pressure x-ray-diffraction studies were performed on Bi_2Te powder in order to explore the universality of the collapse into the high-pressure bcc phase that occurs within the $(Bi_2)_m(Bi_2Te_3)_n$ series. At ambient pressure and temperature the Bi_2Te starts out in the hexagonal phase with the P-3m crystal structure, denoted as Bi_2Te-I, which persists up to 7 GPa. Upon compression near 5 GPa an intermediate phase begins to appear, denoted as Bi_2Te-II. Diffraction peaks belonging to this Bi_2Te-II phase are present in the diffraction patterns up to 17 GPa. However, at 9 GPa a second phase transition begins into the Bi_2Te-III that completes at 17 GPa. Integrated diffraction patterns for the three phases are shown in Fig. 1. Bi_2Te-II has a very broad pressure range where it coexists with either phase I or phase III but only a small 2 GPa window in which it is the only phase observed. Within this small window, we were unable to index the peaks to a structure with a pressure-volume dependence that was consistent with phases I and III. In contrast, the high-pressure Bi_2Te-III can easily be indexed to the bcc (Im-3m) unit cell with $a = 3.747$ Å at $P = 8.8$ GPa, and it is the stable phase at 47 GPa, the highest pressure attained in this study. Fitting the pressure-volume data points to the Vinet EOS [34,35] for phase III we obtain $V_o = 29.88(0.27)$ Å, $B_o = 54.2(5)$ GPa, and $B' = 4.78(\pm 0.32)$. This Bi_2Te-III structure is best understood as a disordered substitutional alloy such that the bismuth and tellurium atoms reside randomly on the ($2a$) site of the bcc structure with occupancies defined by the 2:1 Bi:Te stoichiometry of the sample. This is believed to be due to the similar atomic radii of the two elements and is further enabled by charge transfer as a result of the application of high pressure. This behavior has also been seen in similar materials, such as $(Bi,Sb)_2Te_3$ and Bi_4Te_3 [20,36–38]. Furthermore it seems that the unit-cell volume as a function of pressure for the bcc phase in Bi_2Te follows the same P-V curve as do the above-mentioned two compounds [Fig. 2(a)]. We also note that, concomitant with the phase transformation from phase I to phase III, there is a volume collapse of approximately 9%. The fact that Bi_2Te also collapses into the bcc phase *strongly* suggests that, despite having disparate ground-state phases, the entire $(Bi_2)_m(Bi_2Te_3)_n$ series converges into the bcc phase at high pressures. These structural transformations are ubiquitous across this series, which suggests that there should also be concurrent transformations occurring in the electronic structure as well.

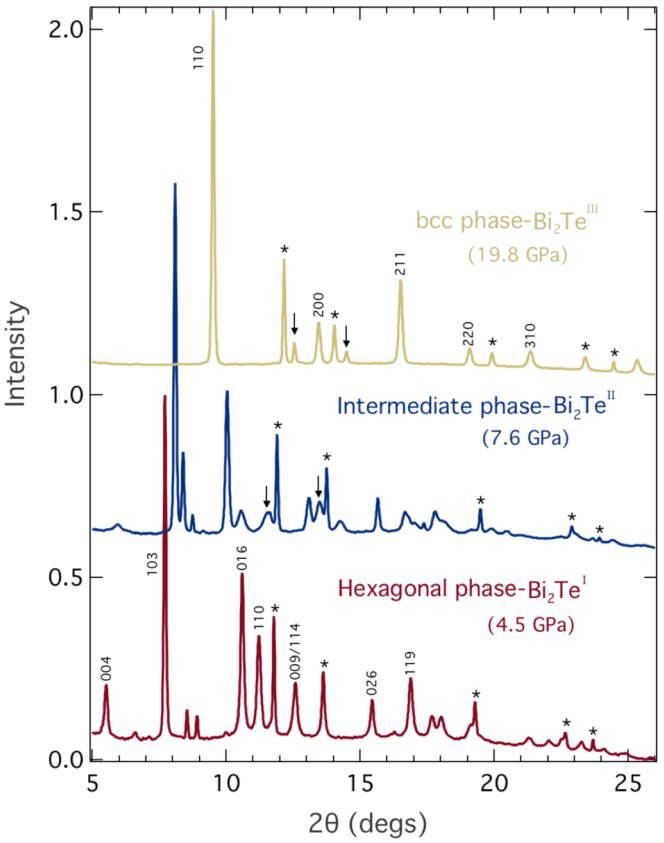

FIG. 1. X-ray-diffraction patterns at pressures within the hexagonal ($P < 5$ GPa), intermediate (5 GPa $< P <$ 17 GPa) and body-centered-cubic phases ($P > 17$ GPa). The *hkl* indices of some of the diffraction reflections are shown for the hexagonal and bcc phases of Bi_2Te. The stars are the peaks from the copper pressure calibrant, and the arrows show the peaks due to the neon pressure medium.

High-pressure magnetotransport measurements were performed to investigate the effects of the high-pressure structural phase transformations on the electronic structure of Bi_2Te. Hall resistance at 25 K as a function of applied magnetic field is shown in Fig. 3 for selected pressures. It can be seen that there is a clear change in the Hall resistance between 5.4 and 7.6 GPa, coincident with the phase transformation from the hexagonal phase (Bi_2Te-I) to the intermediate mixed phase (Bi_2Te-II) observed in x-ray diffraction. Although the structural and electronic phase transitions occur at nearly the same pressure, the difference in the two transition pressures could be attributed to the different pressure media used in the two experiments. The neon gas used in the diffraction measurements is considered hydrostatic up to about 10 GPa

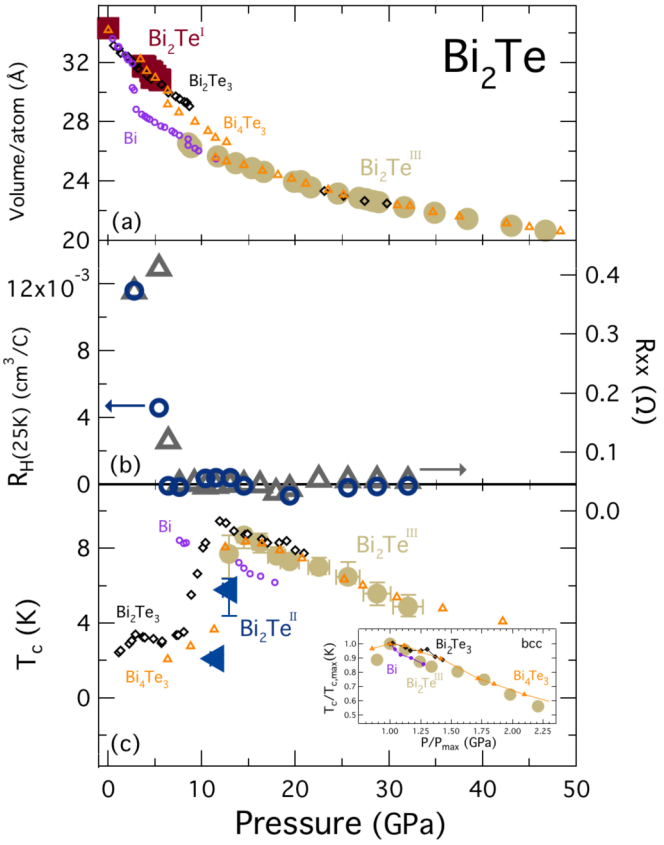

FIG. 2. (a) Bi_2Te shows universal behavior in the high-pressure phase as it collapses into the bcc phase, just as the other members of the infinitely adaptive $(Bi_2)_m(Bi_2Te_3)_n$ series do. This result confirms this family of compounds with disparate electronic and crystal structure ground states can be tuned by the application of pressure to elicit a universal metallic superconducting phase with the body-centered-cubic crystal structure. (b) The electronic phase transitions that accompany the structural transitions are seen in the semimetal to metal crossover near 5 GPa as well as the change in charge-carrier type between 10 and 14 GPa. R_H is given as the slope of the Hall resistance R_{xy} versus the applied magnetic field (Fig. 3). (c) T_c as a function of pressure for Bi_2Te plotted with the other members of the homologous family showing similar trends for peaks of T_c before entering the bcc phase. (The inset) T_c normalized to maximum T_c in the bcc phase to show the same relation of slope for T_c versus pressure in the bcc phase for the entire $(Bi_2)_m(Bi_2Te_3)_n$ series.

[39], whereas the steatite used in the magnetotransport measurements is a solid medium that can support small pressure gradients. Nonetheless, the fact that both phase diagrams agree as well as they do shows that the pressure medium is not affecting the structure or phase transformation mechanisms, although it is worth considering that it may be affecting some subtle electronic properties that are below the resolution of this study. The linearity of R_{xy} as a function of applied magnetic field suggests a dominant carrier type (Fig. 3) for all pressures at $T = 25$ K, but for pressures below 9.2 GPa a multiband picture of Bi_2Te emerges in the temperature dependence of the Hall coefficient (Fig. 4). At 2.8 GPa there is a crossover from a negative to a positive Hall coefficient near 70 K demonstrating

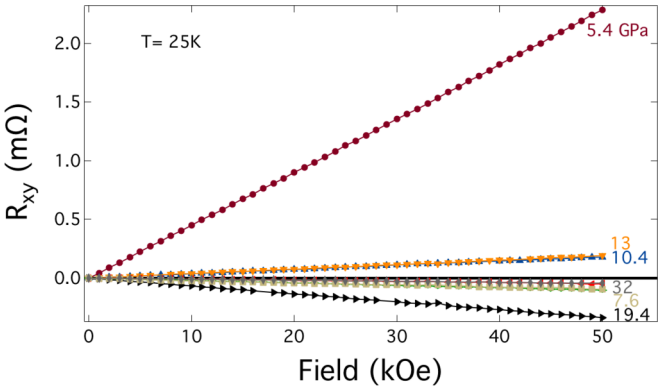

FIG. 3. Hall resistance at 25 K as a function of applied magnetic field for pressures between 5.4 and 32 GPa. There is a significant decrease in the Hall resistance above 5.4 GPa, which indicates a drastic change in the carrier concentration. Also, the change in the sign of the slope indicates that the majority carrier changes as pressure is increased, although the fact that R_{xy} versus H remains linear up to 50 kOe suggests that there is a single dominant charge carrier for all of the pressures studied.

a change in the dominant charge-carrier type. From our x-ray-diffraction measurements we know that Bi_2Te is in a mixed phase regime above 5 GPa, but as pressure is increased above 2.8 GPa the crossover temperature in the Hall sign decreases as does the magnitude of the Hall coefficient, suggesting a net increase in the carrier density as a function of pressure. In the mixed phase above 5.4 GPa there is very little change in the carrier concentration, compared to the concentration in the low-pressure hexagonal phase Bi_2Te-I. This can be clearly seen in Fig. 2(b) where the slope of the Hall resistance versus applied field R_H and the longitudinal resistance R_{xx} are plotted as a function of pressure. The Hall coefficient R_H, as

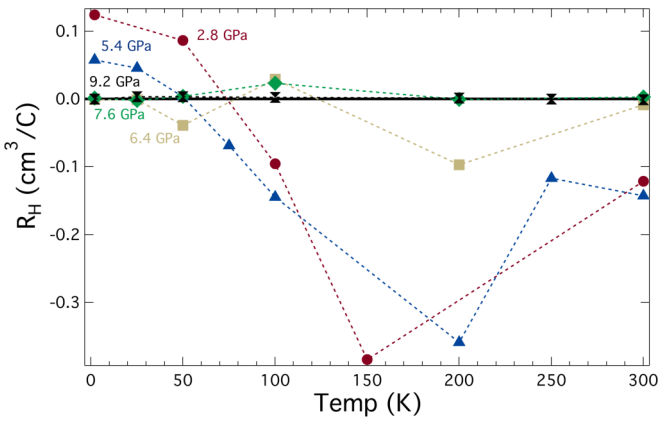

FIG. 4. Hall coefficient (linear fit to the data shown in Fig. 3) plotted as a function of temperature at increasing pressures shows the suppression of the carrier crossover from near 70 K at 2.8 GPa to 50 K at 5.4 GPa until it is nearly flat by 7.6 GPa with no visible change in carrier as a function of temperature. Although it is difficult to interpret these results given that the system is in the intermediate mixed phase region above 5 GPa, this figure shows that both temperature and pressure [Fig. 2(b)] affect the band structure of Bi_2Te and drive it from a semimetal to a metal via two separate tuning parameters.

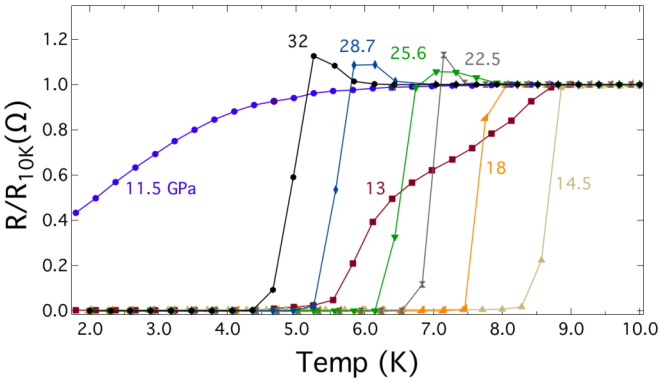

FIG. 5. Resistance as a function of temperature for pressures from 11.5 to 32 GPa showing the onset and subsequent suppression of the superconducting state in Bi_2Te. The resistance is normalized to the value of the resistance at 10 K for each particular pressure just to emphasize the change in T_c as a function of pressure.

defined above as the slope of the Hall resistance as a function of applied magnetic field, is inversely proportional to the carrier density and, if the carrier concentrations are calculated using a single band model, there is an increase in carrier concentration within order of magnitude from $\sim 10^{21}\,\mathrm{cm}^{-3}$ at 2.8 GPa—more typical of a semimetal—to $\sim 10^{23}\,\mathrm{cm}^{-3}$ for pressures of 6.4 GPa and above—more characteristic of a typical metal. Considered within the single band model, this suggests that there is a metallization of Bi_2Te at these higher pressures and there should now be more electrons available to form superconducting pairs as has been seen in many of the other members of the $(Bi_2)_m(Bi_2Te_3)_n$ series [17,18,20].

Low-temperature high-pressure transport data (Fig. 5) show the onset of superconductivity at 11.5 GPa. Although Bi_2Te did not fully enter the superconducting state by our minimum temperature of 1.8 K, we can extrapolate that the midpoint of the transition should have a $T_c \cong 2.1$ K (see Fig. 5). At the next pressure of $P = 12.9$ GPa, there are two transitions visible as it enters the superconducting state. This correlates with the fact that the system is in the intermediate Bi_2Te-II and Bi_2Te-III mixed phase with a different T_c's for the two states [see Fig. 2(c)]. T_c increases sharply between 11.5 and 12.9 GPa for both transitions with $T_{c,II} = 5.8$ and $T_{c,III} = 7.7$ K. Once the pressure is increased to $P = 14.5$ GPa there is a single sharp superconducting transition, which gives the maximum $T_c = 8.6$ K with a transition width of only 0.57 K. Although from the x-ray-diffraction data we know that Bi_2Te is still in the mixed phase at $P = 14.5$ GPa, the superconducting transition seems dominated by the Bi_2Te-III (bcc) phase and has a T_c similar to the maximum T_c of Bi [17], Bi_4Te_3 [20] (both 8.4 K), and Bi_2Te_3 [18] (9.3 K) under pressure, all of which transform into a high-pressure bcc phase. After reaching its maximum, T_c decreases monotonically down to $T_c = 4.9$ K at 32 GPa.

The universality of the superconducting state of the $(Bi_2)_m(Bi_2Te_3)_n$ series in the high-pressure bcc phase can be seen more clearly by plotting the reduced critical temperature $T_c/T_{c,\max}$ versus $P/P_{c,\max}$, where $P_{c,\max}$ is the pressure where $T = T_{c,\max}$, as is shown in the Fig. 2(c) inset. This shows the linear trend common to the series as T_c is suppressed by increasing pressure after reaching $T_{c,\max}$ at a rate of $dT_c/dP = -0.34 \pm 0.02$ K GPa. The linear suppression of T_c is consistent with BCS-type phonon-mediated superconductivity in Bi_2Te in which pressure raises the average phonon frequency and reduces the electron-phonon coupling, thus decreasing the pairing mechanism strength [40,41]. To further investigate the nature of the superconducting state using a treatment consistent with a BCS superconducting state, we can look at the electron-phonon coupling through the McMillan formula to find the volume Grüneisen parameter and compare it with other BCS superconductors.

The McMillan formula is given as $T_c = (\langle\omega\rangle/1.2)\exp\{[-1.04(1+\lambda)]/[\lambda - \mu^*(1+0.62\lambda)]\}$, valid in the strong-coupling regime ($\lambda \leqslant 1.5$) and connects T_c with the electron-phonon coupling parameter λ, an average phonon frequency $\langle\omega\rangle$, and the screened Coulomb repulsion μ^* (taken here to be 0.1) [42]. By taking the logarithmic volume derivative of T_c, we get the relation,

$$\frac{d\ln T_c}{d\ln V} = -\gamma + \Delta\left\{\frac{d\ln\eta}{d\ln V} + 2\gamma\right\},$$

in which $\gamma = -d\ln\langle\omega\rangle/d\ln V$ is the Grüneisen parameter, $\eta = N(E_f)\langle I^2\rangle$ is the Hopfield parameter, which is given by the product of the electronic density of states and the average-squared electronic matrix element, and $\Delta = 1.04\lambda[1+0.38\mu^*]/[\lambda - \mu^*(1+0.62\lambda)]^2$ [43]. Although the average phonon frequency $\langle\omega\rangle$ has not been determined experimentally for Bi_2Te at high pressures, we can test a range of values of 100, 200, and 300 K that cover the range of the typical values. We choose $P = 14.5$ GPa, where T_c is a maximum at 8.6 K, to look at these values. Substituting $T_c = 8.6$, $\langle\omega\rangle = 100$ K, and $\mu^* = 0.1$ into the McMillan equation and solving for λ, we find $\lambda = 1.17$. We can then substitute this value into the equation for Δ, which gives a value of $\Delta = 1.28$. All of these values can then be substituted into the above equation to find γ. We can extract the value of $d\ln T_c/d\ln V$ from our experimental data by combining our equation of state data [Fig. 4(a)] with the superconducting phase diagram [Fig. 4(c)]. If we plot $\ln T_c$ versus $\ln V$ and take the derivative near $P = 14.5$ GPa, we find a value of $d\ln T_c/d\ln V = 5.55\,\mathrm{K\,\AA}^3$. Substituting this value into the above equation for γ, along with our value of Δ, and taking the value of $d\ln\eta/d\ln V = -1$ [44], assuming again that Bi_2Te behaves like a simple p-electron metal, we are able to extract a value of $\gamma = 4.38$. To test the parameters of this calculation we can vary the value of $\langle\omega\rangle = 200$ and 300 K, which gives values of $\gamma = 2.3$ and 1.9, respectively, closer to that of tin (Sn) ($\gamma \approx +2.1$) [45]. While yielding a γ value closer to that expected for simple metals, such as Sn, $\langle\omega\rangle = 200$ or 300 K are substantially higher values than that of Sn ($\langle\omega\rangle \approx 110$ K) [42]. Given the strong compression of the lattice at the pressures where superconductivity is observed, it is likely that there is commensurate phonon stiffening, which would serve to increase $\langle\omega\rangle$. In light of this potential phonon stiffening, a value of $\langle\omega\rangle = 200$ K does not seem unreasonable, and therefore the associated γ may be a reasonable estimate. Even with uncertainties in $\langle\omega\rangle$, the γ values calculated for Bi_2Te suggest that it behaves like a simple BCS-type phonon-mediated superconductor in the high-pressure bcc phase. Future experiments studying

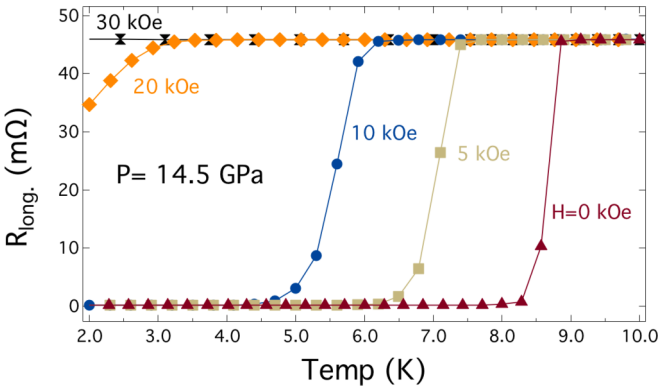

FIG. 6. Suppression of the superconducting transition with magnetic field at $P = 14.5$ GPa shown in plots of resistance as a function of temperature. The linear trend of dT_c/dH can be more clearly seen in the phase diagram shown in Fig. 7.

the high-pressure phonon dispersions in Bi_2Te are needed to determine the actual value of $\langle\omega\rangle$ and thereby more accurately determine the nature of the superconducting state in Bi_2Te and possibly the rest of the homologous series.

To investigate the pair-breaking mechanism in greater detail we applied magnetic fields to study how the superconducting state is suppressed as a function of pressure and magnetic field. This is shown for a single pressure of $P = 14.5$ GPa for applied fields up to 30 kOe (Fig. 6) but was performed at all of the pressures in order to understand the pressure evolution of the superconducting state. Figure 7 shows the rate of suppression of T_c with the applied magnetic field at all pressures up to 32.0 GPa. T_c is defined as the midpoint of the superconducting transition and is only needed to be estimated for the highest applied magnetic fields, except at $P = 28.7$ GPa. The estimated superconducting transition temperatures for the extrapolated data were based on a linear extrapolation of the resistance versus temperature curve for temperatures where $T_{\text{midpoint}} < T_{\text{final}} < T_{\text{onset}}$. The rate of suppression is quasilinear at all pressures down to the lowest temperatures measured. This quasilinear trend of $H_{c2}(T)$ has also been observed in Bi_4Te_3 [20], Bi_2Se_3 [26], $Cu_xBi_2Te_3$

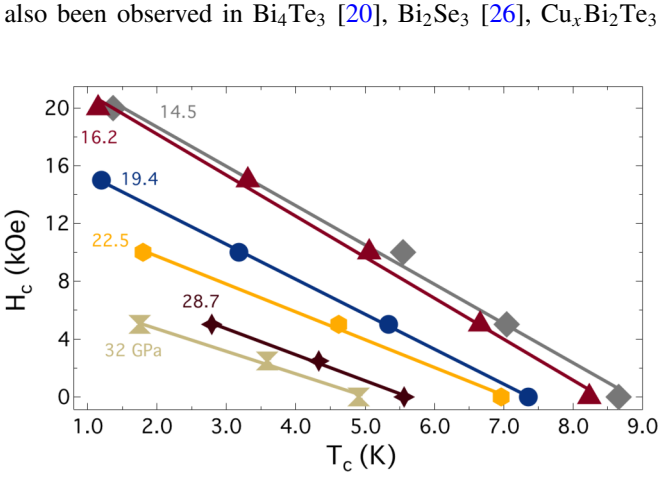

FIG. 7. H_c is suppressed linearly with temperature for all of the pressures studied. T_c is taken to be the midpoint of the superconducting transition. The error bars are smaller than the marker size (see the text).

[46], YPtBi [47,48], and ErPdBi [49]. Considering that all of these materials contain bismuth, these results suggest that strong spin-orbit scattering is the dominant pair-breaking mechanism in these materials.

As a starting point to analyze superconductivity in Bi_2Te we begin by assuming that it is a conventional superconductor. This is supported by the linear suppression of T_c as a function of pressure in Bi_2Te [42]. In fact, the canonical model for this analysis, developed by Werthamer, Helfand and Hohenberg (WHH) [50], was originally applied to a Ti-Nb alloy with a bcc structure, similar to that of Bi_2Te, and contains a parameter which incorporates spin-orbit effects, which are germane to any modeling of Bi-containing systems. Within the WHH model for orbitally limited superconductors we can calculate the upper critical field at $P = 14.5$ GPa as $H_{c2}(0) = -0.7T_c \times dH_{c2}/dT|_{T=T_c} = 1.94$ T where $T_c(H = 0) = 8.66$ K is taken at the midpoint of the superconducting transition, and $dH_{c2}/dt = -0.321$ T K. This is lower than the measured $H_{c2}(2\,K) = 2.12$ T, suggesting that there is another mechanism involved in the superconducting pair breaking. If H_{c2} is Pauli limited, then the superconducting gap energy Δ is equal to the Zeeman energy and therefore the Pauli limiting field $H_P = 1.84T_c = 15.93$ T at $P = 14.5$ GPa. Since the measured H_{c2} is higher than the orbital limit but significantly lower than H_P, we can assume that both orbital and Pauli limiting effects are in play with the orbital mechanism being the dominant one. To incorporate both mechanisms into our calculations of H_{c2}, we can recalculate H_{c2} using the modified formula, which includes the Maki parameter $\alpha = \sqrt{2}H_{c2}^{\text{orb}}/H_p$ [51] so that $H_{c2}^{\alpha} = H_{c2}^{\text{orb}}/\sqrt{(1+\alpha^2)} = 1.79$ T at $P = 14.5$ GPa, where $\alpha = 0.172$,, $H_{c2}^{\text{orb}} = 1.94$ T, and $H_P = 15.93$ T. Including the Maki parameter only lowers the calculated $H_{c2}(T)$, providing further evidence that the pair breaking in Bi_2Te is driven by spin-orbit scattering and not Pauli spin paramagnetism.

To compare our results within the WHH theory for spin-singlet superconductors we plot the normalized critical field $h^*(t) = (H_{c2}/T_c)/|dH_{c2}/dT|_{t=1}$ as a function of the normalized temperature $t = T/T_c$ for selected pressures up to 32 GPa (Fig. 8). The error bars in Fig. 8 are determined by propagating the individual uncertainties (e.g., ΔT_c) in the parameters defining h^* and t. Since we define T_c as the midpoint of the superconducting transition, the error in T_c is defined as the accuracy of the measurement of the resistance at T_c, where $\Delta R/R$ is $\pm 1\%$. Given that the temperature is accurate to $\pm 1\%$, we take whichever is the larger of the two as the error in T_c. Due to trapped magnetic flux within the magnet, there is an uncertainty in the applied field of 0.1 kOe: $\Delta H_{c2} = 0.1$ kOe. The error in $|dH_{c2}/dT|_{t=1}$ is defined from the standard deviation returned from linear fits to the data near $t = 1$. Because the critical field curves exhibit strong linearity, the slope near $t = 1$ can be determined with an error below 2%.

All of the pressures follow the same $h^*(t)$ slope and remain linear down to the lowest temperatures measured at $t \sim 0.3$. Based on the strong spin-orbit effects of Bi-based materials, we assumed that spin-orbit scattering was the main contributor to the pair-breaking mechanisms in Bi_2Te and therefore we include spin-orbit effects (λ_{so}) within the WHH formalism in a similar fashion to Ref. [52] and compare

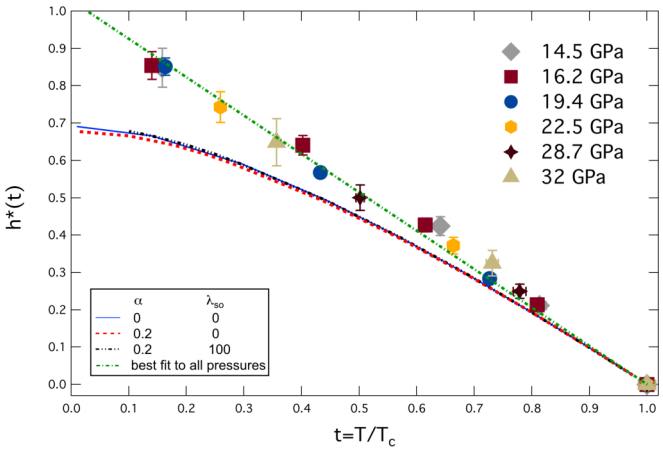

FIG. 8. Graph showing the renormalized $H_{c2}(T)$ for selected pressures using the reduced temperature T/T_c and the reduced critical field (see the text) in order to compare with theory. The fitting is performed using the classical WHH model in which the blue dashed line is the limit of the Maki parameter, $\alpha = 0$ and the spin-orbit scattering strength $\lambda_{so} = 0$. To compare our data with the WHH model we used $\alpha = 0.2$ and varied λ_{so} to see the effect of spin-orbit scattering. As is shown in the figure, due to the fact that α is so small, even with values of λ_{so} up to 100 (well outside of WHH conditions) our data begins to deviate from the models for $t < 0.7$. The error bars are propagated from uncertainties in the measured quantities (see the text).

them to our experimental results (Fig. 8): The blue dashed line is the WHH in the dirty limit ($\alpha = 0$); the red dashed line includes a value of $\alpha = 0.2$ (close to our experimental value of 0.172 calculated for $P = 14.5$ GPa) and $\lambda_{so} = 0$; and the black dashed line includes $\alpha = 0.2$ and an unphysically large $\lambda_{so} = 100$. The addition of $\alpha = 0.2$ shifts the $h^*(t)$ curve down only slightly and only for $t \leqslant 0.3$. Because α is so small in Bi_2Te, increasing λ_{so} barely shifts the $h^*(t)$ curve up even for $\lambda_{so} = 100$, a spin-orbit scattering strength, which is well outside the limits of WHH. Considering that our data deviate from all of these models below $t \sim 0.5$, it is clear that a theory which includes very strong spin-orbit interactions must be developed to deal with this and similar spin-orbit-driven superconductors as attested to by a growing body of experimental work [26,46,48,53].

In conclusion, we have found that Bi_2Te provides further evidence of a universal behavior of the series to collapse into the bcc structure at high pressures. Although Bi_2Te enters a high-pressure mixed phase region between roughly 5 and 17 GPa, we were able to observe a semimetal-metal transition near 5.4 GPa in both linear and Hall resistance measurements. We were able to establish that there is a dominant carrier type below 5.4 GPa via magnetic-field and temperature-dependence measurements, although it was difficult to unambiguously determine carrier type and concentration in the mixed phase. We also discovered pressure-induced superconductivity in Bi_2Te with a maximum $T_c = 8.66$ K at $P = 14.5$ GPa. Bi_2Te has a similar maximum T_c (~8 K) to other materials in the $(Bi_2)_m(Bi_2Te_3)_n$ series as well as a similar rate of suppression of T_c with pressure. Analysis of the pressure dependence of the superconducting state suggests that Bi_2Te is likely a conventional BCS superconductor, but the linear suppression of T_c with the field implies unconventional and strong spin-orbit scattering pair-breaking effects. This pair breaking is outside of the scope of the conventional WHH theory and requires a new treatment that is able to incorporate strong spin-orbit scattering. Although establishing whether Bi_2Te has topologically nontrivial surface states is outside the scope of this paper, as a member of the homologous series $(A_2)_n(A_2B_3)_m$ where $A = Bi, Sb, Pb, Ge$ and $B = Te, Se, S$, many permutations and dopings of these and similar materials [14,15,46,54–56] have produced TIs. It would be of great interest if future work could confirm whether Bi_2Te is a TI via theoretical calculations as well as experimental techniques, such as angle-resolved photoemission spectroscopy, scanning tunneling microscopy, or quantum oscillations. This would help to confirm the universality of the infinitely adaptive $(Bi_2)_m(Bi_2Te_3)_n$ series, not only with regard to the superconducting state and high-pressure crystal structure, but also in the topological nature of these materials.

ACKNOWLEDGMENTS

This work was performed under LDRD (Tracking Code No. 14-ERD-041) and under the auspices of the U.S. Department of Energy (DOE) by Lawrence Livermore National Laboratory (LLNL) under Contract No. DE-AC52- 07NA27344. Portions of this work were performed at HPCAT (Sector 16), Advanced Photon Source (APS), Argonne National Laboratory. HPCAT operations are supported by the DOE-NNSA under Award No. DE-NA0001974 and the DOE-BES under Award No. DE-FG02-99ER45775 with partial instrumentation funding by the NSF. The Advanced Photon Source is a U.S. DOE Office of Science User Facility operated for the DOE Office of Science by Argonne National Laboratory under Contract No. DE-AC02-06CH11357. Beam time was provided by the Carnegie DOE-Alliance Center (CDAC). Y.K.V. acknowledges support from DOE-NNSA Grant No. DE-NA0002014.

[1] M. Z. Hasan and C. L. Kane, Colloquium: Topological insulators, Rev. Mod. Phys. **82**, 3045 (2010).

[2] S.-Y. Xu, I. Belopolski, N. Alidoust, M. Neupane, G. Bian, C. Zhang, R. Sankar, G. Chang, Z. Yuan, C.-C. Lee, S.-M. Huang, H. Zheng, J. Ma, D. S. Sanchez, B. Wang, A. Bansil, F. Chou, P. P. Shibayev, H. Lin, S. Jia, and M. Z. Hasan, Discovery of a Weyl fermion semimetal and topological Fermi arcs, Science **349**, 613 (2015).

[3] H. Weyl, Elektron und gravitation. I, Z. Phys. **56**, 330 (1929).

[4] C. L. Kane and E. J. Mele, Z_2 Topological Order and the Quantum Spin Hall Effect, Phys. Rev. Lett. **95**, 146802 (2005).

[5] J. E. Moore and L. Balents, Topological invariants of time-reversal-invariant band structures, Phys. Rev. B **75**, 121306 (2007).

[6] L. Fu and C. L. Kane, Superconducting Proximity Effect and Majorana Fermions at the Surface of a Topological Insulator, Phys. Rev. Lett. **100**, 096407 (2008).

[7] A. Y. Kitaev, Fault-tolerant quantum computation by anyons, Ann. Phys. (N.Y.) **303**, 2 (2003).

[8] F. Wilczek, Majorana returns, Nat. Phys. **5**, 614 (2009).

[9] B. A. Bernevig, T. L. Hughes, and S.-C. Zhang, Quantum spin Hall effect and topological phase transition in HgTe quantum Wells, Science **314**, 1757 (2006).

[10] M. König, S. Wiedmann, C. Brüne, A. Roth, H. Buhmann, L. W. Molenkamp, X.-L. Qi, and S.-C. Zhang, Quantum spin Hall insulator state in HgTe quantum Wells, Science **318**, 766 (2007).

[11] D. Hsieh, Y. Xia, L. Wray, D. Qian, A. Pal, J. H. Dil, J. Osterwalder, F. Meier, G. Bihlmayer, C. L. Kane, Y. S. Hor, R. J. Cava, and M. Z. Hasan, Observation of unconventional quantum spin textures in topological insulators, Science **323**, 919 (2009).

[12] Y. Xia, D. Qian, D. Hsieh, L. Wray, A. Pal, H. Lin, A. Bansil, D. Grauer, Y. S. Hor, R. J. Cava, and M. Z. Hasan, Observation of a large-gap topological-insulator class with a single Dirac cone on the surface, Nat. Phys. **5**, 398 (2009).

[13] J. W. G. Bos, H. W. Zandbergen, M. H. Lee, N. P. Ong, and R. J. Cava, Structures and thermoelectric properties of the infinitely adaptive series $(Bi_2)_m(Bi_2Te_3)_n$, Phys. Rev. B **75**, 195203 (2007).

[14] R. J. Cava, H. Ji, M. K. Fuccillo, Q. D. Gibson, and Y. S. Hor, Crystal structure and chemistry of topological insulators, J. Mater. Chem. C **1**, 3176 (2013).

[15] Y. Ando, Topological insulator materials, J. Phys. Soc. Jpn. **82**, 102001 (2013).

[16] S. Scherrer and H. Scherrer, in *CRC Handbook of Thermoelectrics*, edited by D. M. Rowe (CRC, Boca Raton, FL, 1995).

[17] M. A. Ilina and E. S. Itskevich, Superconductivity of Bismuth Telluride, Fiz. Tverd. Tela **13**, 2496 (1971).

[18] C. Zhang, L. Sun, Z. Chen, X. Zhou, Q. Wu, W. Yi, J. Guo, X. Dong, and Z. Zhao, Phase diagram of a pressure-induced superconducting state and its relation to the Hall coefficient of Bi_2Te_3 single crystals, Phys. Rev. B **83**, 140504 (2011).

[19] Y. L. Chen, J. G. Analytis, J.-H. Chu, Z. K. Liu, S.-K. Mo, X. L. Qi, H. J. Zhang, D. H. Lu, X. Dai, Z. Fang, S. C. Zhang, I. R. Fisher, Z. Hussain, and Z.-X. Shen, Experimental realization of a three-dimensional topological insulator, Bi_2Te_3, Science **325**, 178 (2009).

[20] J. R. Jeffries, A. L. Lima Sharma, P. A. Sharma, C. D. Spataru, S. K. McCall, J. D. Sugar, S. T. Weir, and Y. K. Vohra, Distinct superconducting states in the pressure-induced metallic structures of the nominal semimetal Bi_4Te_3, Phys. Rev. B **84**, 092505 (2011).

[21] K. Matsubayashi, T. Terai, J. S. Zhou, and Y. Uwatoko, Superconductivity in the topological insulator Bi_2Te_3 under hydrostatic pressure, Phys. Rev. B **90**, 125126 (2014).

[22] A. Nakayama, M. Einaga, Y. Tanabe, S. Nakano, F. Ishikawa, and Y. Yamada, Structural phase transition in Bi_2Te_3 under high pressure, High Pressure Res. **29**, 245 (2009).

[23] G. Parthasarathy and W. B. Holzapfel, High-pressure structural phase transitions in tellurium, Phys. Rev. B **37**, 8499 (1988).

[24] F. P. Bundy and K. J. Dunn, Pressure Dependence of Superconducting Transition Temperature of High-Pressure Metallic Te, Phys. Rev. Lett. **44**, 1623 (1980).

[25] Y. Akahama, M. Kobayashi, and H. Kawamura, Structural phase transitions in selenium up to 150 GPa, Jpn. J. Appl. Phys., Part 1 **32**, 22 (1993).

[26] K. Kirshenbaum, P. S. Syers, A. P. Hope, N. P. Butch, J. R. Jeffries, S. T. Weir, J. J. Hamlin, M. B. Maple, Y. K. Vohra, and J. Paglione, Pressure-Induced Unconventional Superconducting Phase in the Topological Insulator Bi_2Se_3, Phys. Rev. Lett. **111**, 087001 (2013).

[27] P. P. Kong, J. L. Zhang, S. J. Zhang, J. Zhu, Q. Q. Liu, R. C. Yu, Z. Fang, C. Q. Jin, W. G. Yang, X. H. Yu, J. L. Zhu, and Y. S. Zhao, Superconductivity of the topological insulator Bi_2Se_3 at high pressure, J. Phys.: Condens. Matter **25**, 362204 (2013).

[28] A. P. Hammersley, S. O. Svensson, M. Hanfland, A. N. Fitch, and D. Hausermann, Two-dimensional detector software: From real detector to idealised image or two-theta scan, High Pressure Res. **14**, 235 (1996).

[29] A. Dewaele, P. Loubeyre, and M. Mezouar, Refinement of the equation of state of tantalum, Phys. Rev. B **69**, 092106 (2004).

[30] S. T. Weir, J. Akella, C. Aracne-Ruddle, Y. K. Vohra, and S. A. Catledge, Epitaxial diamond encapsulation of metal microprobes for high pressure experiments, Appl. Phys. Lett. **77**, 3400 (2000).

[31] D. Jackson, J. Jeffries, W. Qiu, J. Griffith, S. McCall, C. Aracne, M. Fluss, M. Maple, S. Weir, and Y. Vohra, Structure-dependent ferromagnetism in Au4V studied under high pressure, Phys. Rev. B **74**, 174401 (2006).

[32] G. J. Piermarini, S. Block, J. D. Barnett, and R. A. Forman, Calibration of pressure-dependence of R1 ruby fluorescence line to 195 kbar, J. Appl. Phys. **46**, 2774 (1975).

[33] W. L. Vos and J. A. Schouten, On the temperature correction to the ruby pressure scale, J. Appl. Phys. **69**, 6744 (1991).

[34] P. Vinet, J. Ferrante, J. R. Smith, and J. H. Rose, A universal equation of state for solids, J. Phys. C: Solid State Phys. **19**, L467 (1986).

[35] P. Vinet, J. Ferrante, J. H. Rose, and J. R. Smith, Compressibility of Solids, J. Geophys. Res. [Solid Earth Planets] **92**, 9319 (1987).

[36] L. Zhu, H. Wang, Y. Wang, J. Lv, Y. Ma, Q. Cui, Y. Ma, and G. Zou, Substitutional Alloy of Bi and Te at High Pressure, Phys. Rev. Lett. **106**, 145501 (2011).

[37] J. G. Zhao, H. Z. Liu, L. Ehm, Z. Q. Chen, S. Sinogeikin, Y. S. Zhao, and G. D. Gu, Pressure-induced disordered substitution alloy in Sb_2Te_3, Inorg. Chem. **50**, 11291 (2011).

[38] M. Einaga, A. Ohmura, A. Nakayama, F. Ishikawa, Y. Yamada, and S. Nakano, Pressure-induced phase transition of Bi_2Te_3 to a bcc structure, Phys. Rev. B **83**, 092102 (2011).

[39] S. Klotz, J. C. Chervin, P. Munsch, and G. L. Marchand, Hydrostatic limits of 11 pressure transmitting media, J. Phys. D: Appl. Phys. **42**, 075413 (2009).

[40] W. L. McMillan, Transition temperature of strong-coupled superconductors, Phys. Rev. **167**, 331 (1968).

[41] J. Bardeen, L. N. Cooper, and J. R. Schrieffer, Theory of superconductivity, Phys. Rev. **108**, 1175 (1957).

[42] R. C. Dynes, McMillan's equation and the Tc of superconductors, Solid State Commun. **10**, 615 (1972).

[43] J. J. Hopfield, On the systematics of high Tc in transition metal materials, Physica **55**, 41 (1971).

[44] J. S. Schilling and S. Klotz, in *Physical Properties of High Temperature Superconductors III*, edited by D. M. Ginsberg (World Scientific, Singapore, 1992), p. 59.

[45] A. Eiling and J. S. Schilling, Pressure and temperature dependence of electrical resistivity of Pb and Sn from 1–300 K and 0–10 GPa-use as continuous resistive pressure monitor accurate over wide temperature range; superconductivity under pressure in Pb, Sn and In, J. Phys. F: Met. Phys. **11**, 623 (1981).

[46] Y. S. Hor, A. J. Williams, J. G. Checkelsky, P. Roushan, J. Seo, Q. Xu, H. W. Zandbergen, A. Yazdani, N. P. Ong, and R. J. Cava, Superconductivity in $Cu_xBi_2Se_3$ and Its Implications for Pairing in the Undoped Topological Insulator, Phys. Rev. Lett. **104**, 057001 (2010).

[47] N. P. Butch, P. Syers, K. Kirshenbaum, A. P. Hope, and J. Paglione, Superconductivity in the topological semimetal YPtBi, Phys. Rev. B **84**, 220504 (2011).

[48] T. V. Bay, T. Naka, Y. K. Huang, and A. de Visser, Superconductivity in noncentrosymmetric YPtBi under pressure, Phys. Rev. B **86**, 064515 (2012).

[49] Y. Pan, A. M. Nikitin, T. V. Bay, Y. K. Huang, C. Paulsen, B. H. Yan, and A. de Visser, Superconductivity and magnetic order in the noncentrosymmetric half-Heusler compound ErPdBi, Europhys. Lett. **104**, 27001 (2013).

[50] N. R. Werthamer, E. Helfand, and P. C. Hohenberg, Temperature and purity dependence of the superconducting critical field, Hc2. III. Electron spin and spin-orbit effects, Phys. Rev. **147**, 295 (1966).

[51] K. Maki, Effect of Pauli paramagnetism on magnetic properties of high-field superconductors, Phys. Rev. **148**, 362 (1966).

[52] Y. Lu, T. Takayama, A. F. Bangura, Y. Katsura, D. Hashizume, and H. Takagi, Superconductivity at 6 K and the violation of Pauli limit in $Ta_2Pd_xS_5$, J. Phys. Soc. Jpn. **83**, 023702 (2014).

[53] T. Klimczuk, K. Baroudi, J. W. Krizan, A. L. Kozub, and R. J. Cava, Superconductivity in the niobium-rich compound Nb_5Se_4, J. Alloys Compd. **649**, 906 (2015).

[54] S. V. Eremeev, G. Landolt, T. V. Menshchikova, B. Slomski, Y. M. Koroteev, Z. S. Aliev, M. B. Babanly, J. Henk, A. Ernst, L. Patthey, A. Eich, A. A. Khajetoorians, J. Hagemeister, O. Pietzsch, J. Wiebe, R. Wiesendanger, P. M. Echenique, S. S. Tsirkin, I. R. Amiraslanov, J. H. Dil, and E. V. Chulkov, Atom-specific spin mapping and buried topological states in a homologous series of topological insulators, Nat. Commun. **3**, 635 (2012).

[55] K. Govaerts, M. H. F. Sluiter, B. Partoens, and D. Lamoen, Homologous series of layered structures in binary and ternary Bi-Sb-Te-Se systems: *Ab initio* study, Phys. Rev. B **89**, 054106 (2014).

[56] T. Valla, H. Ji, L. M. Schoop, A. P. Weber, Z.-H. Pan, J. T. Sadowski, E. Vescovo, A. V. Fedorov, A. N. Caruso, Q. D. Gibson, L. Müchler, C. Felser, and R. J. Cava, Topological semimetal in a $Bi\text{-}Bi_2Se_3$ infinitely adaptive superlattice phase, Phys. Rev. B **86**, 241101 (2012).